Chapter 2

Numerical Welding Simulation as a Basis for Structural Integrity Assessment of Structures: Microstructure and Residual Stresses

Kimiya Hemmesi and Majid Farajian

Additional information is available at the end of the chapter

http://dx.doi.org/10.5772/intechopen.74466

Abstract

The importance of welding process modeling is specifically related to the role of the induced welding residual stresses and distortions on the structural behavior of the components under service load. In the absence of reliable information on the magnitude and distribution of residual stresses, it is generally assumed that residual stresses are as high as the yield strength of the material that could lead to overconservatism in design and consequently economic challenges. The more exact the microstructure and residual stress or strain fields is predicted, the better one can judge the risk of structural damage, for example, the formation of fatigue cracks or initiation of failure. In this chapter, the application of finite element approach to the calculation of welding residual stresses is described through three different case studies. SYSWELD has been used for welding simulation. Residual stress measurements are carried out to determine the distribution of residual stresses in three orthogonal directions, on the surface and in the bulk of the material. The numerical results are compared directly with the measured data. The overall aim is to evaluate the use of finite element approach in the accurate calculation of residual stress states for use in the structural integrity assessments.

Keywords: welding simulation, residual stresses, finite element method (FEM), X-ray diffraction, neutron diffraction

1. Introduction

In fusion welding, concentrated heat is injected into the joint locally and is dissipated into the weldments, leading to an inhomogeneous temperature field in the welded material.

The maximum temperature in this time-dependent field reaches beyond the melting point in the weld pool, and the minimum value is the ambient temperature being reached after cooling down. Within this temperature field and due to the temperature-dependent physical and mechanical properties, an inhomogeneous thermal stress field is generated. The thermal stresses can either be accommodated elastically or lead to a stress state in which plastic deformations would be inevitable. There is another source of plastic deformation, which is induced during solid-state phase transformations if phase transformation occurs. As a result of the inhomogeneous plastic deformation during welding, some regions do not fit into the space available, and due to geometrical compatibility, a residual stress field arises.

The reliable characterization of welding residual stresses in structural components has been widely considered in many research communities. Tensile residual stresses which are present in welds could potentially decrease the tolerance of the component against applied external loads. In integrity assessments, the interaction between load and residual stresses is taken into account by using a couple of conservative approaches [1]. In order to predict the more realistic service life of welded components, it is necessary to be aware of the residual stress fields, particularly in the critical crack initiation sites. Over the past few decades, a large number of researches have been devoted to the experimental and numerical determination of welding residual stresses. Recent advances in both simulation and measurement of weld residual stresses have provided the possibility to describe the residual stresses. However, owing to the different thermal, metallurgical, and mechanical complexities and the interaction between them, there still exist a number of uncertainties in the accurate calculation and measurement of residual stresses. On the other hand, it is extremely difficult to quantify separately the effects of several variables and parameters.

1.1. Computational welding mechanics

Experimental analysis for the determination of the residual stress fields in welds by means of nondestructive methods requires complementary diffraction instruments [2]. Such studies are very costly, and because of the limitation of the volume and mass of the investigated object, they could just provide one in best case information about a portion of the whole residual stress field in a large structure. A scientific and engineering approach to solve this problem is the application of numerical methods for describing the development of residual stresses and studying their behavior under different mechanical and thermal loads.

Welding as a multi-physics problem is one of the most complicated processes from the modeling point of view. Different aspects, namely the arc physics, transient heat transfer, conductivity, fluid flow, phase transformations, grain size and deformations must be taken into account into the model. The first works on application of the numerical analysis of welds and the behavior of the material during welding are those of Boulton [3] and Rosenthal [4]. Since then, many models for the description of the heat source have been developed, which are all mentioned in the literature survey by Goldak [5].

In most models, which are used for the calculation of residual stress and distortion, the real heat input is simulated via an equivalent substitute heat source moving in the direction of welding. The fluid dynamics in the weld pool are almost always not included.

http://dx.doi.org/10.5772/intechopen.74466

Residual stress and distortion are strongly influenced by the temperature-dependent plasticity. In **Figure 1**, the thermomechanical processes for the development of welding stresses are schematically illustrated. Here in this model from Radaj [6], the plastic zones in front and a linear heat source in a quasi-stationary temperature field are shown. The drawn parabola-like curve separates the heated front area which is due to the thermal stresses under compression from the rear region which is under tensile stresses. The zone of elastic unloading is located between the two areas. The cyclic plasticity at the shown locations in the base material, the heat affected zone and the weld during the heating and cooling phases show how the residual stresses develop. Point 1 undergoes elastic compressive stress, and at point 2, a plastic deformation occurs after reaching the compressive yield strength before this point is elastically relieved at point 3. The permanent elongation by compression at point 3 could lead to tensile residual stresses after cooling. Points 4 and 5 experienced tensile stresses during cooling due to the shrinkage restraint.

The remaining strain at point 5 may indicate that after reaching room temperature, compressive residual stresses may be present. Point 6 would have a mechanical load cycle as point 5, if it would not have been so close to the heat source. Point 7 is on the weld center and is only subjected to elasto-plastic tensile stresses. It is understandable that the temperature-dependent spatial and temporal process and material modeling determine the accuracy of the residual stress and distortion calculations.

Computational welding mechanics is an engineering subject concerned with the mechanics and the material behavior during welding. In research and applications, the different welding processes, the microstructures resulting in the weld and their mechanical properties in terms of deformability, strength, and toughness and the structural behavior of welded components are to be considered for an advanced fitness-for-service assessment of welded components.

The accuracy of the predicted results in the calculation of residual stresses as a complex nonlinear problem is influenced by several assumptions and simplifications. Nevertheless, the experimental measurement of welding residual stresses involves a significant range of uncertainties. Since both numerical and experimental approaches involve inevitably their own limitations, it is necessary to apply these methods in combination with each other.

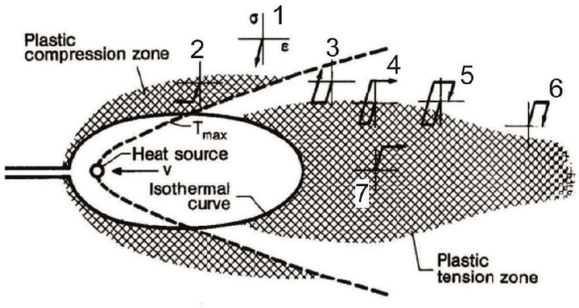

Figure 1. Cyclic plasticity in the weld, heat-affected zone and the base material and the formation of welding residual stresses [6].

With the development of modern high speed computers, process modeling has become a powerful tool for controlling and optimizing of different process parameters. Nowadays, finite element method has contributed in process simulation extensively. In the context of weld computational mechanics, modern software infrastructures, that is, the physics, mechanics, materials science, mathematics and numerical algorithms have been enriched enough to allow complex calculation of welded structures [7]. A proper FE model for welding simulation involves advanced aspects such as definition of the heat source, material phase transformations, temperature-dependent thermophysical and mechanical properties and material hardening behavior. But the key issue in this regard is to understand the underlying theory well enough. In the study described here, it has been tried to handle as much as possible the various assumptions and simplifications in the prediction of welding residual stresses.

In this chapter, three fusion weld case studies are described with focus on different geometries, single or multiple pass welds and finally different types of base materials particularly with regard to metallurgical behavior and hardening behavior. As the first case study [8], under the support of German Research Foundation (DFG) [9], a tubular specimen made of S355J2H structural steel was utilized for the weld residual stress assessments. The specimen was manufactured under closely controlled conditions. After the preparations, a single-pass dummy weld without filler material was created in the specimen. Appropriate material characterization was performed on the base metal under static and cyclic loading conditions. In the case studies two [10] and three [11], the results of a scientific community, the international *Network on Neutron Techniques standardization for Structural Integrity* (NeT) will be discussed. This network consists of 15 European-based member research institutes, universities and industries, which meet twice a year and discuss the results of defined round-robin tasks on welding simulation and experimental residual stress measurement techniques. Within the framework of NeT round robin, case study two focuses on a single bead on plate made of austenitic stainless steel and finally case study three deals with the multipass welding of Inconel.

Nickel alloy similar to stainless steel is a face-centered cubic, which shows no phase transformation during cooling from its melting temperature down to the room temperature. Thus, cooling rate for both stainless steel and nickel alloy is of less importance. However, for nickel alloys, particularly the precipitation hardened alloys, the composition-related metallurgical effects should be taken into account. Nickel alloys compared with stainless steels have lower thermal expansion coefficient, which may cause less distortion problems. The procedures for welding of stainless steels and nickel alloys are relatively similar. Sequentially, coupled thermal-mechanical analyses were performed in both task groups. The accuracy of predictions for the transient temperature field, welding residual stresses, equivalent plastic strains, and so on was then calibrated based on experimental measurements. The achievements and results could be then used as lessons for further numerical simulation. This involves the global calibration of the heat input on the basis of the thermocouple responses and detailed determination of the heat source parameters by matching the weld fusion boundaries to real weld cross sections.

Different stages of calculation were compared with experimental tests by taking into account the limitations and uncertainties of the measurements. In the thermo-metallurgical

http://dx.doi.org/10.5772/intechopen.74466

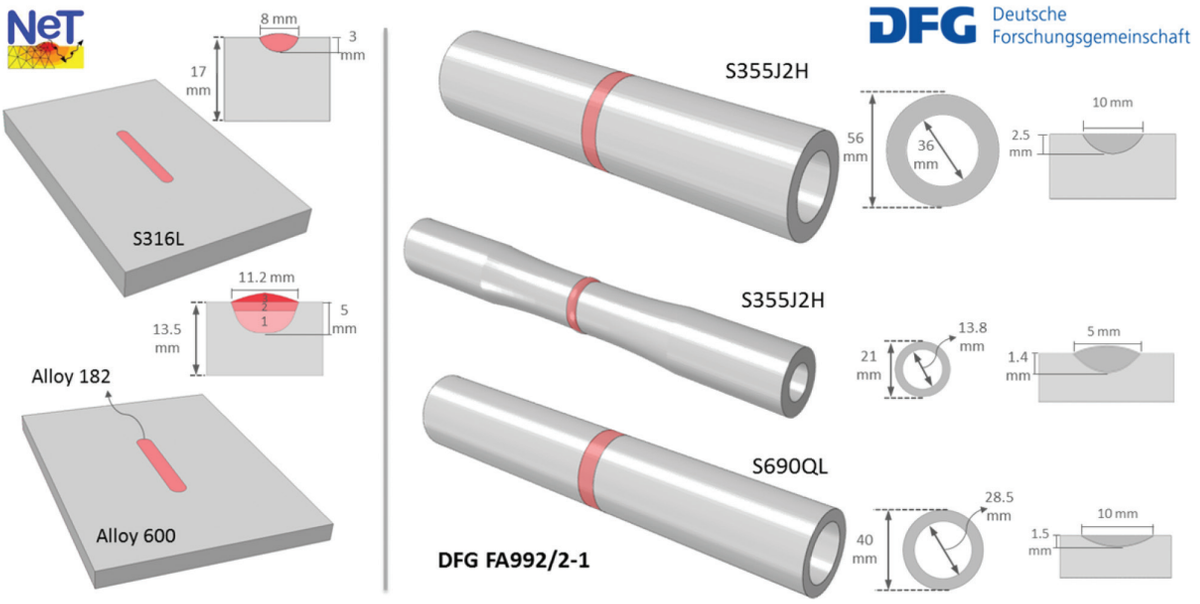

Figure 2. Simulation studies and residual stress measurements: cooperation in NeT (left), investigations within the project by German Research Foundation (DFG) (right).

phase, the transient temperature history during the welding process was calibrated by means of the measured thermocouple profiles. Furthermore, the fusion boundary of the weld bead was controlled by the cross-sectional macrograph of the specimen. Once an accurate thermo-metallurgical solution is obtained, one can study the mechanical aspect of the weld calculation. One of the most important focuses on the mechanical solution as the next step is to determine the best explanatory material hardening model. Since the predicted residual stresses are sensitive strongly to the high-temperature mechanical properties and especially to the cyclic hardening parameters, it is important to consider all the possible material-related simulation variables. The accuracy of calculated residual stresses was then controlled with measured data in order to optimize the choices for different variables. Since it is preferred to make use of through-thickness stress profiles for structural integrity and defect tolerance assessments [1], both X-ray and neutron diffraction measurement techniques were used in order to describe the surface and depth profile of welding residual stresses.

For all the calculations, the FEM weld-specific program SYSWELD was used as simulation tools (**Figure 2**).

2. Numerical studies of welding residual stresses

The accurate structural integrity assessment of welded structures or components requires the designers to be aware of the existing welding residual stress field within the material. A complex process such as welding could be described by means of both numerical and experimental techniques.

In this chapter, the applicability of FEM to the simulation of welding process is being examined. Three-dimensional models were applied within the commercial software package SYSWELD 8.5 to calculate numerically the inevitable residual stress field, which is produced as a consequence of nonuniform heating and cooling. A coupled thermo-metallurgical simulation was then conducted and the results of which included temperature history and phase proportions. These were then used as the input for further mechanical analyses within the uncoupled simulation technique. Using this technique, though the insignificant dimensional changes as well as the mechanical work are neglected, the accuracy of the results is kept to a high level. Different aspects of numerical welding simulation are explained in detail in Ref. [8].

2.1. Case study 1: S355J2H single bead on tube

On the basis of the well-documented experimental results on tubular specimens made of S355J2H in the project DFG FA992/1–1 [9], extensive numerical studies on welding simulation were performed on this material. The key modeling issues were as follows: heat source representation, solid-state phase transformation kinetic, material hardening laws and temperature-dependent material behavior. In the thermo-metallurgical phase, the transient temperature history during the welding process was calibrated according to the measured responses from the thermocouples along with the cross-sectional macrographs from the weld fusion boundaries. Once an accurate thermo-metallurgical solution was obtained, the mechanical aspects of the welding simulation were considered. Temperature dependent material properties together with cyclic hardening parameters are two important material related simulation variables which must be taken into account since they may affect strongly the predicted residual stresses. The accuracy of the calculated residual stress field was then validated by means of X-ray and neutron diffraction measurements.

2.1.1. Welded specimens

The tubular specimens out of structural steel S355J2H had a length of 250 mm with the outside and inside diameter of 56 and 36 mm, respectively. The base metal before welding had been heat treated for 30 min at 600°C under shielding gas in order to relieve the existing machining-induced residual stresses. The samples were produced by means of Tungsten Inert Gas (TIG) welding without filler material (**Figure 3**). The arc voltage, welding current and welding speed were set to 12 V, 250A and 15 cm/min, respectively, providing a total input energy of 7.2 kJ/cm. In this way, a 10 mm wide and 2.5 mm deep weld bead was produced on every tube. NiCr-Ni thermocouples were used to measure the temperature history at every 90^{o} around the weld toe (Q1–Q4) [12].

2.1.2. Plasticity and material hardening model

Von Mises yield function is considered in this work as the criterion to describe where the plastic deformation begins. Besides that, the constitutive behavior of the material and the respective hardening model must be defined properly in order to preserve the accuracy of the calculated residual stresses. For simplicity, a single-element FE analysis technique was then applied in order to investigate the influence of the chosen hardening model on the predicted stress-strain responses of the material under mechanical loading conditions. In this regard, the calculation

http://dx.doi.org/10.5772/intechopen.74466

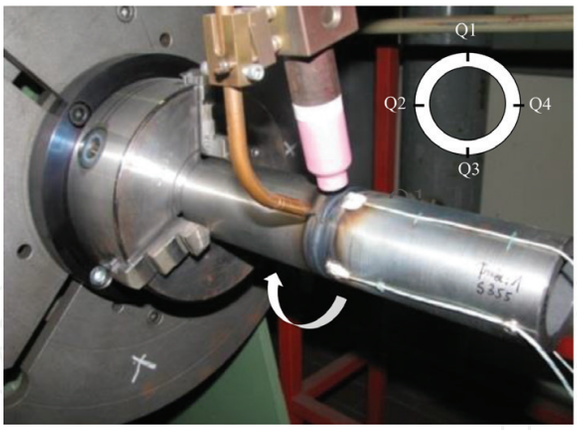

Figure 3. TIG welding of the tubular specimens with temperature measurements [8].

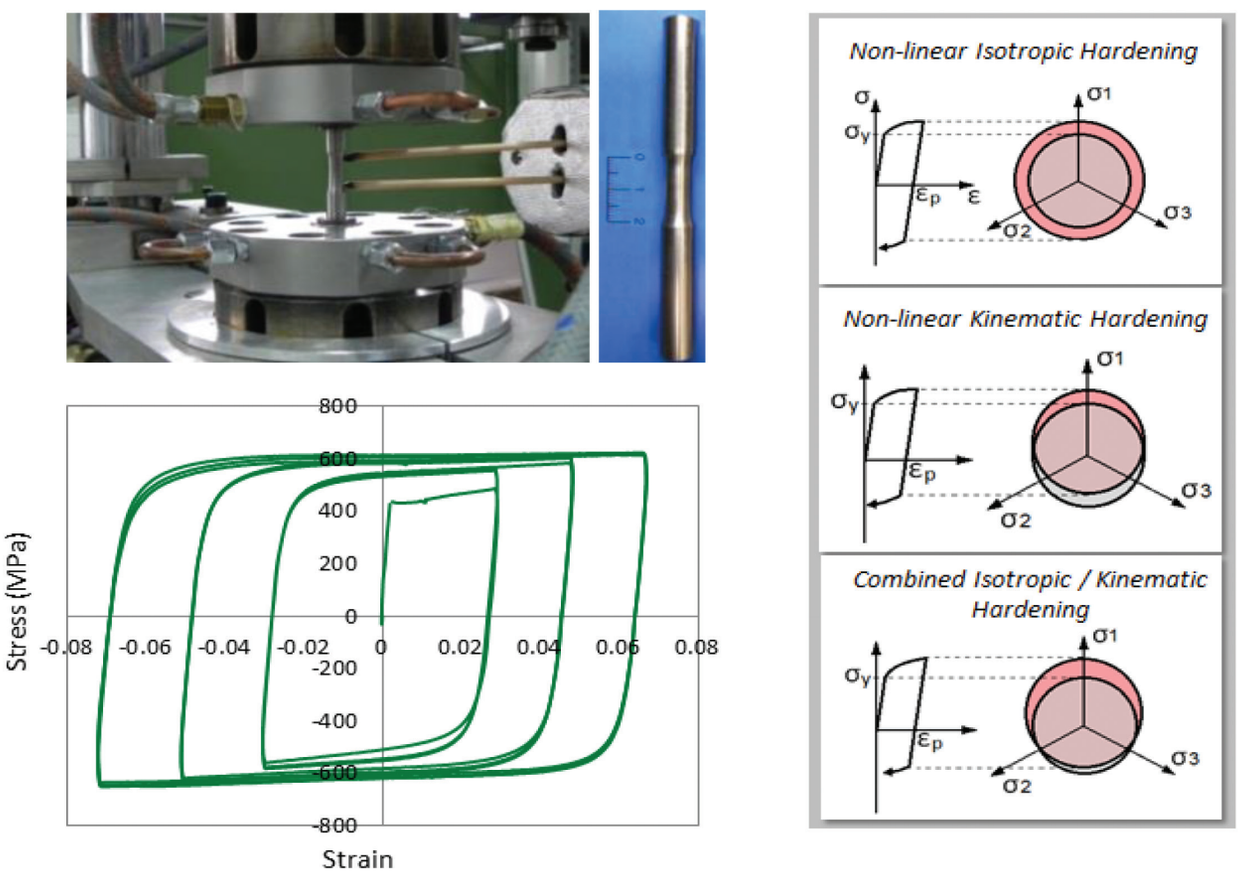

Figure 4. Low cycle fatigue test results of S355J2H at $\Delta\varepsilon = 0.06$, 0.1 and 0.14 (left), different types of hardening model [8].

results under symmetric strain-controlled cyclic loading were compared with the obtained stress-strain responses from the isothermal low cyclic fatigue tests at constant amplitude. Three process-related strain ranges, namely 6%, 10% and 14% were chosen for the LCF tests as shown in **Figure 4**.

SYSWLED supports the modeling of the nonlinear kinematic hardening behavior in the form of Armstrong-Frederick combined hardening model [13] under the isothermal and monophasic condition:

$$\acute{\sigma}\left(\varepsilon_{eq}^{p}\right) = \acute{\sigma}_{0}\left(\varepsilon_{eq}^{p}\right) + \frac{C}{\gamma}\left(1 - e^{-\gamma\varepsilon_{eq}^{p}}\right) \quad (1)$$

where $\acute{\sigma}$ represents $\sigma - \sigma_0$ and σ_0 is the yield stress at zero plastic strain, ε_{eq}^{p} is the equivalent plastic strain and C and γ are material kinematic hardening parameters (supported only as a single pair for this model). Isotropic hardening component that defines the expansion of the yield surface as a function of accumulated plastic strain is represented through the σ'_0 term. Meanwhile, the kinematic hardening component is introduced to the model to describe the translation of the yield surface in the stress space.

In order to define the kinematic hardening parameters, the model could be fitted in different ways to either monotonic or uniaxial cyclic stress-strain curves. Two case studies were considered in this work. In case 1, whether a pure kinematic or a combined isotropic-kinematic hardening model is implemented, the kinematic behavior is assumed to be linear. In this regard, the maximum plastic strain for defining the monotonic true stress versus plastic strain response was set to 100%. In case 2, a nonlinear kinematic hardening behavior was taken into account for both pure kinematic or combined hardening models. In this case, the first cyclic response of the material taken from the LCF test data was used in order to calibrate the respective model

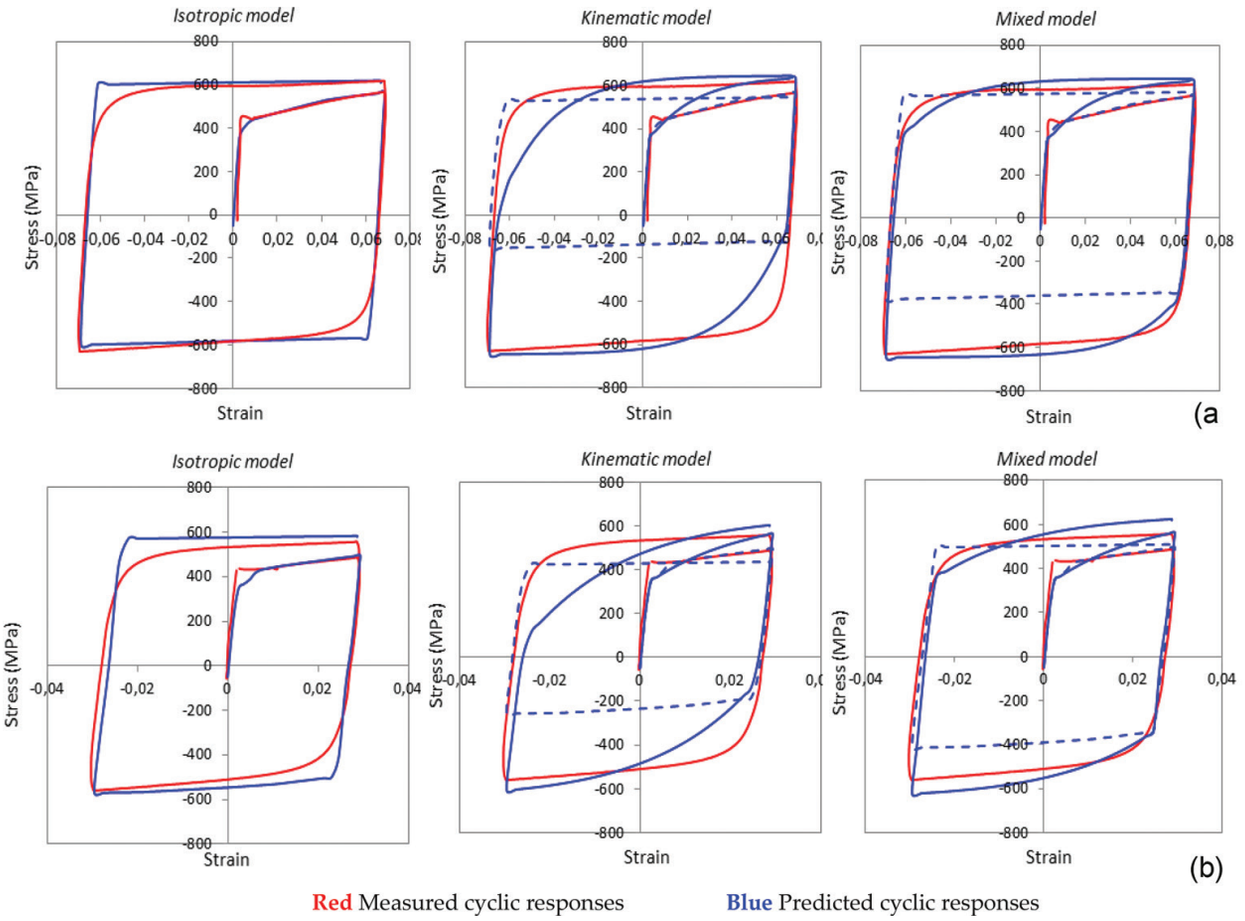

Figure 5. Comparison between the measured and predicted stress-strain responses of S355J2H during the first load reversal at room temperature for strain ranges Δε=0.14 (top) and Δε=0.06 (bottom). Continuous and dashed lines are related to case studies 1 and 2 for finding the kinematic parameters [8].

parameters through the fitting procedure. The total strain range in the respective LCF test was set to 14%. Being a one-pass weld is the cause for choosing the first load reversal as for the fitting procedure. In this case, any extra cyclic hardening is ignored. **Figure 5** shows the predicted responses at two of the strain ranges (6 and 14%) for simple isotropic, pure kinematic and combined isotropic-kinematic hardening models. Red and blue plots in **Figure 5** represent the measured and predicted responses, respectively. The dashed or continuous blue plots refer back to the used fitting approaches for defining the kinematic hardening parameters. In this regard, dashed blue lines and continuous blue line represent case 1 and case 2, respectively. As can be seen in **Figure 5** using the pure isotropic hardening model, though the Bauschinger effect is neglected, the predicted and measured monotonic responses as well as the peak stress values of the cyclic responses agree reasonably well except that the predicted yielding points during the cyclic responses are sharper than the measured ones. In case of using a pure kinematic hardening model, the reversed yielding points were predicted to be much lower than the measured ones due to the incorporation of the Bauschinger effect. In this regard, the nonlinear kinematic hardening model gives obviously better results in predicting the shape and peaks of the hysteresis loops but poorer results in predicting the monotonic stress-strain responses of the material rather than linear one. It should be noted that the level of peak stresses predicted by the linear kinematic hardening model depends strongly on the predefined maximum plastic strain in the monotonic mechanical property. By using the combined isotropic-kinematic hardening model with a 50% isotropic proportion, the reversed yielding points were improved significantly comparing with the pure kinematic cases. Even in the case of combined hardening, if the kinematic model parameters are obtained by fitting to the cyclic stress-strain curves, the predicted monotonic responses do not conform to the experimental curves though the cyclic responses match well enough. Indeed, matching both monotonic and cyclic responses is difficult, which could influence the final results differently depending on the case of study.

2.1.3. Residual stress results

The calculated and measured residual stress fields in the axial and hoop directions at 180º from the weld start point (Q3) are shown in **Figure 6**. As can be seen, the numerical results conform very well the experimentally measured data. Residual stress measurements by means of neutron diffraction (ND) were conducted at Helmholtz-Zentrum Berlin (HZB).

To be able to interpret the formation of welding residual stresses numerically, different aspects of the simulation need to be explained in detail. It is obvious that during welding every material point in the specimen is experiencing different thermal history depending on its location relative to the welded area. In this regard, the evolution of different material phases, cumulative and equivalent plastic strains and finally the welding residual stresses are investigated through the numerical analysis at different positions with respect to the welded area (**Figure 7**). For instance, at node-1, which is located within the welded area, the temperature goes beyond the melting point during heating and thus austenite transformation occurs substantially since the maximum temperature exceeds the austenitization finish temperature (Ac3).

Then, the material cools down from the maximum temperature and the austenite starts to transform into bainite and martensite depending on the cooling rate. The evolution of different

phases during heating and cooling is shown in **Figure 8a**. In **Figure 8b**, the evolution of the axial and hoop residual stresses, the cumulative plastic strain and the equivalent plastic strain are shown by dividing the total process time into seven smaller time intervals. During time intervals 1 and 2, the moving torch does not yet reach Q3; thus, the material at node-1 undergoes some tension and compression elastically. Once the welding torch reaches Q3, the local temperature starts to increase during the time interval 3 and the material undergoes expansion-induced compressive stresses. Since yielding occurs in this period, plastic strain begins to accumulate in the material. In the interval 4 during which the temperature goes beyond 1300°C, the stress components and the cumulative plastic strains disappear since the temperature exceeds the material annealing temperature, which was previously set to 1300°C. Unexpectedly, the equivalent plastic strain is retained as can be seen in **Figure 8b**. Time interval 5 represents the cooling phase from annealing temperature down to bainitic transformation temperature. In this period, tensile stresses appear due to the shrinkage of the material at the point of interest. Meantime, plastic strains start to accumulate again in this period. By further cooling in the time interval 6, austenite starts to transform to bainite since the temperature has dropped below the bainitic transformation temperature. This type of transformation is associated with the decrease of density, which causes volume expansion and thus local compression in the material. Below 420°C in the time interval 7, rest of the austenite phase transforms into martensite, which is associated with more volume increase and consequently the compressive stresses increase. During the time intervals 6 and 7, the strain hardening of the material vanishes gradually due to the hardening recovery phenomena caused by austenite to ferrite transformation.

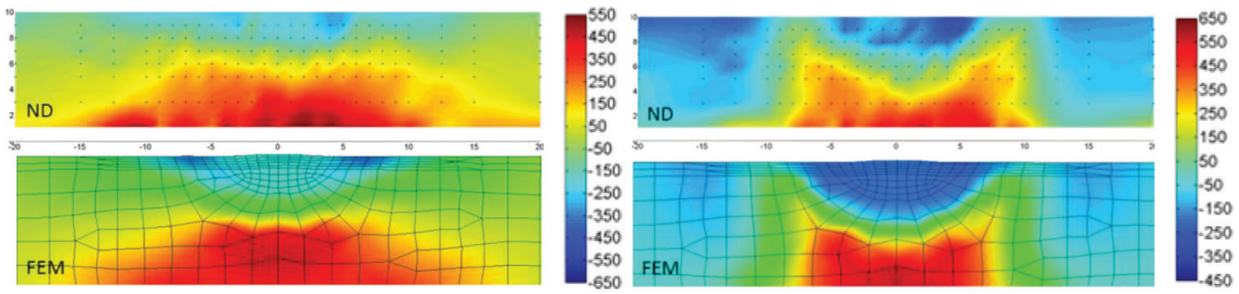

Figure 6. Comparison of the calculated axial (left) and hoop (right) residual stress fields at Q3 with the ND-measurements [8].

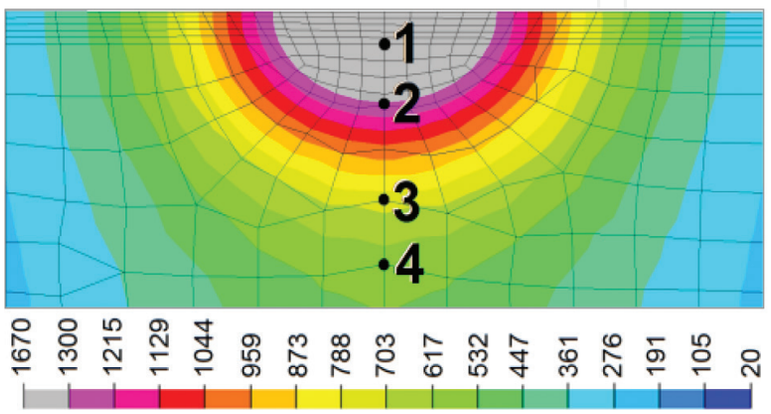

Figure 7. Different representative material zones in the weld cross-section from the FE model at Q3 [8].

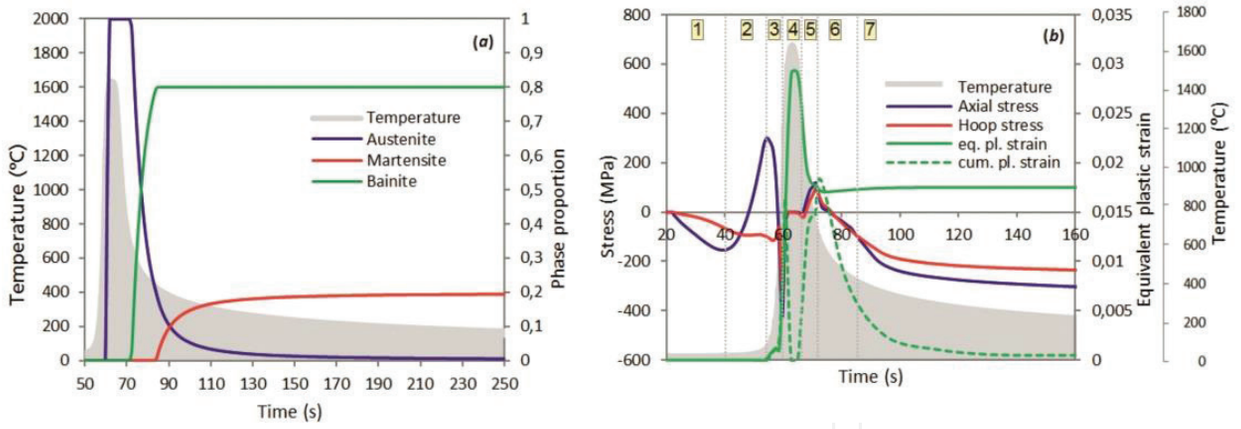

Figure 8. Evolution of different material phases (a) and residual stresses, cumulative and equivalent plastic strains (b) at node-1 with respect to the relevant temperature history [8].

The situation at nodes 2 to 4 differs from what is explained at node-1 regarding the formation of thermal stresses or plastic strains, which is discussed in detail in Ref. [8].

2.2. Case study 2: 316 L single bead on plate

A single weld bead on plate made of austenitic stainless steel was chosen as the benchmark problem for NeT Task Group 1 (TG1) in order to examine the influence of different simulation variables on the accuracy of predicted residual stresses. The specimen geometry and its boundary condition during welding are shown in **Figure 9**. The plate was 17 mm thick and was 200 mm and 150 mm in length and width, respectively. A single TIG weld bead with the same material as the base metal and a width of 7 mm was laid on the surface of the plate. The heat input and welding speed were set to 633 J/mm and 2.27 mm/s, respectively. Both base material and weld metal were characterized using temperature-dependent monotonic and cyclic mechanical tests. For calibration reason, a number of thermocouples were applied to the specimen top and bottom surfaces, along the weld line and as close as possible to the weld. After welding, residual stress measurements were also performed at different locations of the plate by using different techniques such as hole-drilling, contour method and neutron diffraction technique [10]. In TG1, the Bayesian average of the residual stress results from different measurements was used for the calibrations.

2.2.1. NeT TG1 simulation results

A three-dimensional finite element model was developed, and the welding simulations were conducted through sequentially coupled thermal-mechanical solutions. A moving heat source with the Goldak [14] formulation was applied to the model in order to simulate the movement of the welding torch. The gradual material deposition was also included in the model. The annealing scheme was incorporated in the model by considering a melting temperature of 1400°C. In this way, the material history including stress and strain as well as the strain hardening would be eliminated above the annealing temperature.

The heat input energy was calibrated first according to the responses of nine thermocouples [10]. After that, parameters of the heat source were adjusted according to the cross-sectional macro-graphs of the weld in order to match the boundaries of the calculated melted area with the real condition (**Figure 10**).

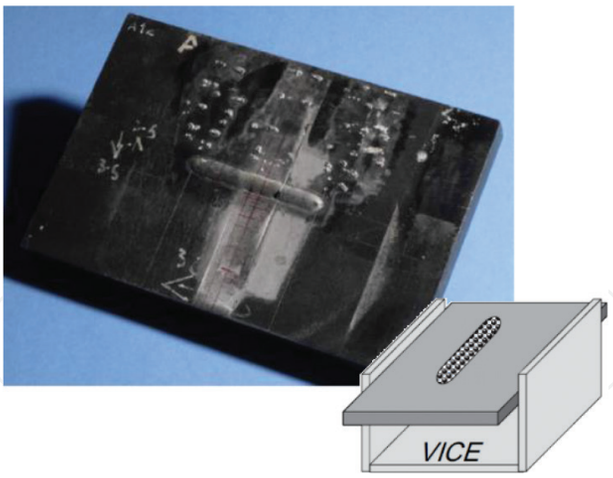

Figure 9. NeT TG1 specimen.

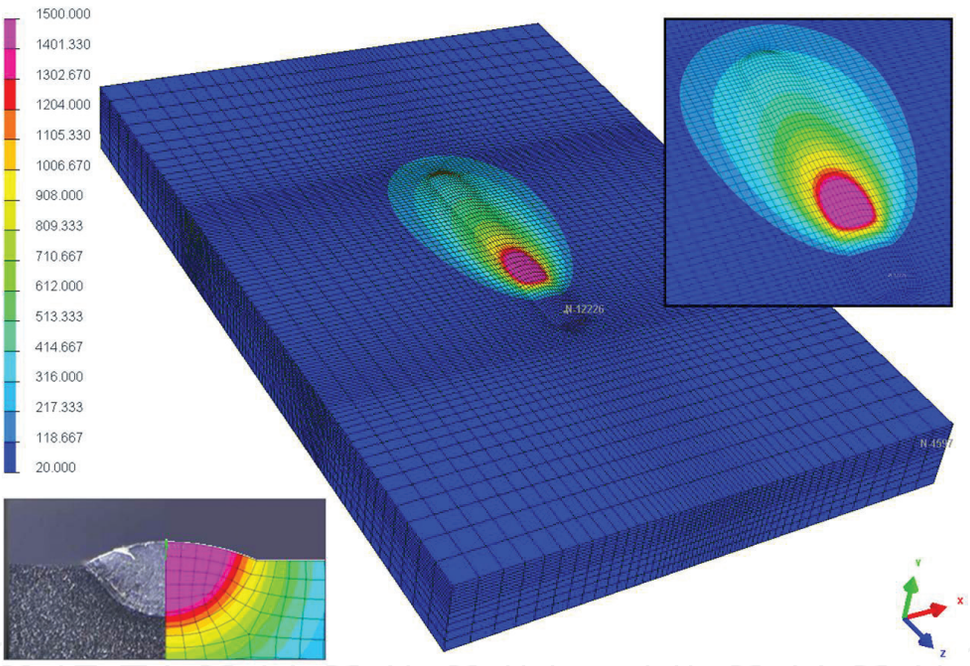

Figure 10. NeT TG1 weld bead on plate simulation.

One of the most important features of NeT TG1 was to comprehensively investigate the influence of material hardening model on the final field of predicted residual stresses. Of course the choice of the hardening model depends strongly on the used material. In this study, isotropic, kinematic and combined isotropic-kinematic hardening models were examined for the welding simulations. For determining the material kinematic hardening parameters, different fitting strategies were adopted, which have been described comprehensively in Ref. [10]. **Figure 11** shows the through thickness variation of transverse residual stresses in the mid-plane. As can be seen, the use of the isotropic hardening model in the welding simulation of the austenitic stainless steel has caused over conservatism in the predicted residual stresses. Combined isotropic-kinematic hardening model has given the best agreement with the experimental results.

http://dx.doi.org/10.5772/intechopen.74466

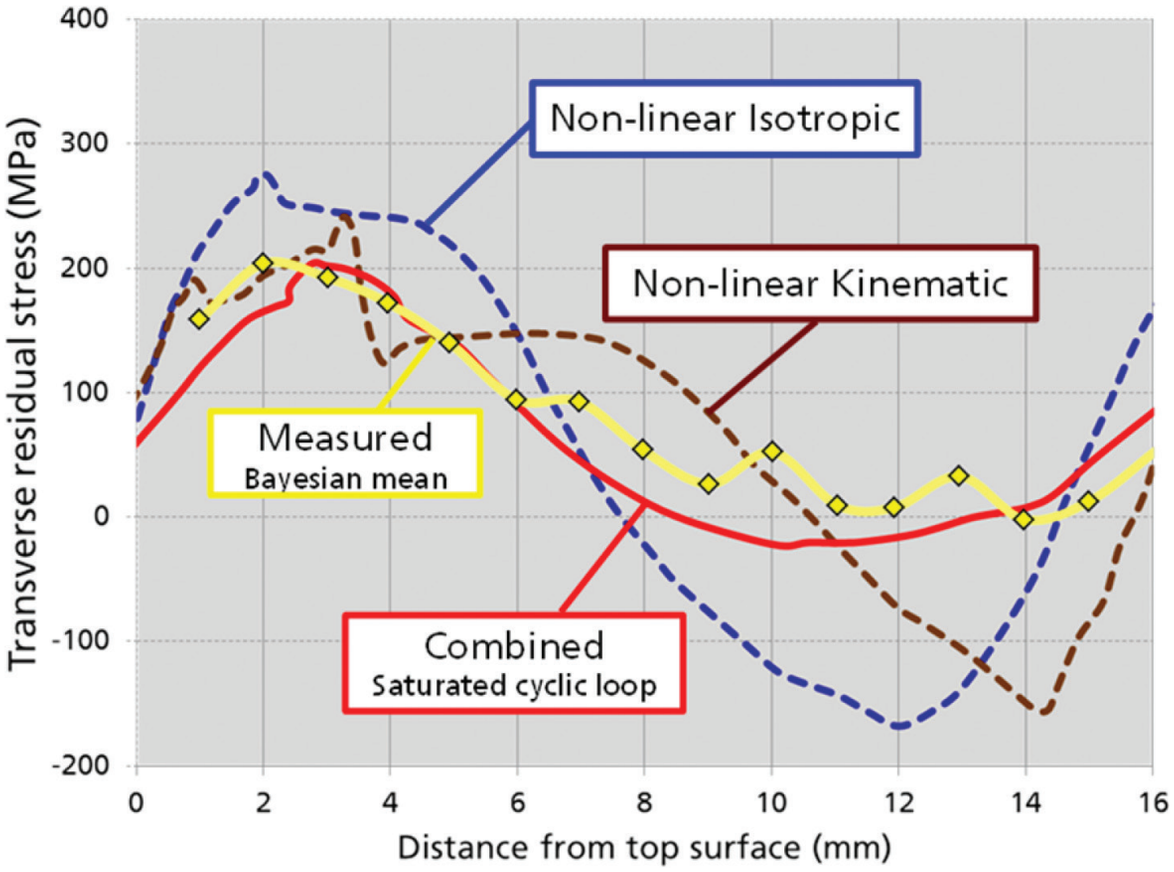

Figure 11. Comparison between the residual stress results using different material hardening models [11].

It should be noted that the yellow curve in **Figure 11** is representative of the Bayesian average of different measured data obtained from different techniques, which were comparable to each other. The combined hardening model in this case is optimized by matching to the saturated cyclic response of the material. In this project, it was observed that other mechanical solution variables than temperature-dependent material properties and material hardening behavior have minor influence on the finial simulation results. Experiences and lessons of NeT TG1 were then collected together as a simulation strategy for the future works and task groups. These lessons are summarized as follows:

- In welding simulation, before proceeding to mechanical simulation, a verified global heat input and a calibrated heat source are absolutely necessary.
- The use of kinematic and combined hardening models or preferably elasto-viscoplastic material constitutive behavior is recommended for the welding simulations.
- The used material constitutive model for the weld metal could differ from that of base material.

2.3. Case study 3: nickel alloy three-pass bead-in-slot

A three-pass slot weld in nickel alloy 600 plate has been chosen as the case study of NeT Task Group 6 (TG6). The dimensions of the plate are 200 mm × 150 mm × 12 mm. The slot is 76 mm

long and 5 mm deep, which was filled with filler material made of alloy 82 (or 182) using the TIG welding process. The welding voltage ranges from 10 to 13 V depending on the weld pass number. Welding current and speed were set to 220 A and 70 mm/min for every pass. The specimen was constrained weakly to allow for free deformations. The multipass welding condition in this study provides complex thermomechanical loading condition, which requires more detailed assumptions and considerations regarding the cyclic behavior of the material. As noted in the NeT TG6 simulation protocol [11], the residual stress measurement is more challenging for the nickel-based alloys as compared with the stainless steel AISI 316. The objective of the NeT TG6 round robin is to promote parallel simulations and measurements in order to accurately predict the welding residual stresses in the slot welds.

2.3.1. Experimental work

A wide range of experiments were performed within the activities of NeT TG6 to support the numerical simulations:

2.3.1.1. Material characterization

The chemical composition, temperature-dependent tensile monotonic and uniaxial cyclic properties of alloy 600 and alloy 82 were determined in the NeT TG6 measurement round robin. Thermomechanical tests using the Gleeble testing machine were performed to determine the properties of the material in the heat-affected zone. LCF test results for alloy 600 at room temperature and 700°C are shown in **Figure 12**. For alloy 182 (weld metal), it was observed that the cyclic hardening rate is lower than the AISI 316 L. Thus, the combined isotropic-kinematic hardening model could be replaced simply with the pure kinematic one. Based on the test results, although the 0.2% proof stresses for the base material and the weld

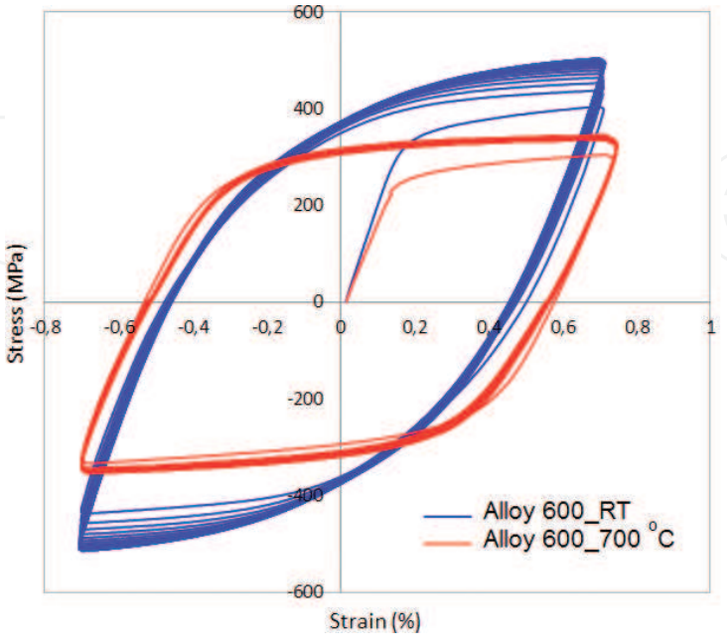

Figure 12. LCF test results for alloy 600 at room temperature and 700°C ($\Delta\varepsilon_{tot}$ = 1.5%).

metal are similar, their work hardening rates are different. Combined hardening (Lemaitre-Chaboche) or pure nonlinear kinematic hardening models were then fitted to the available experimental data in order to determine the model parameters.

2.3.1.2. Hardness measurement

Transverse hardness mapping after producing every single pass is shown in **Figure 13**. As can be seen, the hardness of the weld area is lower than base material.

2.3.1.3. Temperature measurement

A total number of 10 thermocouples were attached to the specimen top and bottom surfaces and close to the weld line. The global heat input and dwell times could be then calibrated on the basis of thermocouples responses. The specimen geometry and the configuration of thermocouples are shown in **Figure 14**.

2.3.1.4. Residual stress measurement

Three sets of neutron diffraction measurements, one set of X-ray diffraction as well as one set of contour method measurements were planned in order to define experimentally the residual stress field in the material. Different sets of measured residual stresses agree well with each other.

2.3.2. Numerical simulations

The simulation methodology used for the welding simulation of nickel alloys is similar to that of AISI 316 L. Lessons and recommendations of NeT TG1 are supposed to be applied in the

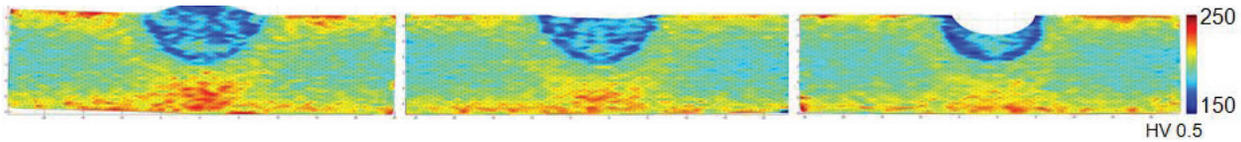

Figure 13. Measured hardness field after finishing each pass.

Figure 14. Specimen geometry and location of the thermocouples close to the slot.

TG6 solutions. Some of these recommendations were mentioned in Section 2.2.1. A preliminary finite element thermal calculation has been performed in Fraunhofer IWM as one of the simulation partners in NeT TG6 round robin. **Figure 15** depicts the comparison between the calculated temperature history and the response of a mid-length thermocouple called TC2.

The agreement between the results is quite well. The criterion for an accurate thermal simulation (as the basic prerequisite for residual stress calculation) is to achieve an agreement with the mid-length thermocouple response within 10%. On the other hand, the calculated melting boundaries including the cross-sectional area and shape of the fusion zone should match the real condition within ±20%. According to **Figure 16**, the calculated fusion boundaries match quite well to the real weld cross section illustrated in the macrographs.

The variation of calculated residual stress components along line BD (through the thickness) and B2 (across to the weld) are shown in **Figure 17** in comparison with the measured results. These results are obtained from neutron diffraction measurements. As can be seen, there exists a reasonable agreement between the calculations and measured results. The existing discrepancy might be attributed to the high-temperature annealing behavior, which is neglected in this study.

As shown in **Figure 17** (top), the maximum amount of longitudinal residual stress along line BD is predicted to be close to the bottom surfaces. According to **Figure 17** (bottom), relatively high tensile residual stresses exist in the weld area and HAZ. A peak value of 500 MPa in the longitudinal direction was observed at the weld toe, which could increase the probability of crack formation at the stress concentration sites, particularly because the most serious cracking problem with nickel alloys is hot cracking in either the weld metal or close to the fusion line in the HAZ with the latter being the more frequent [11].

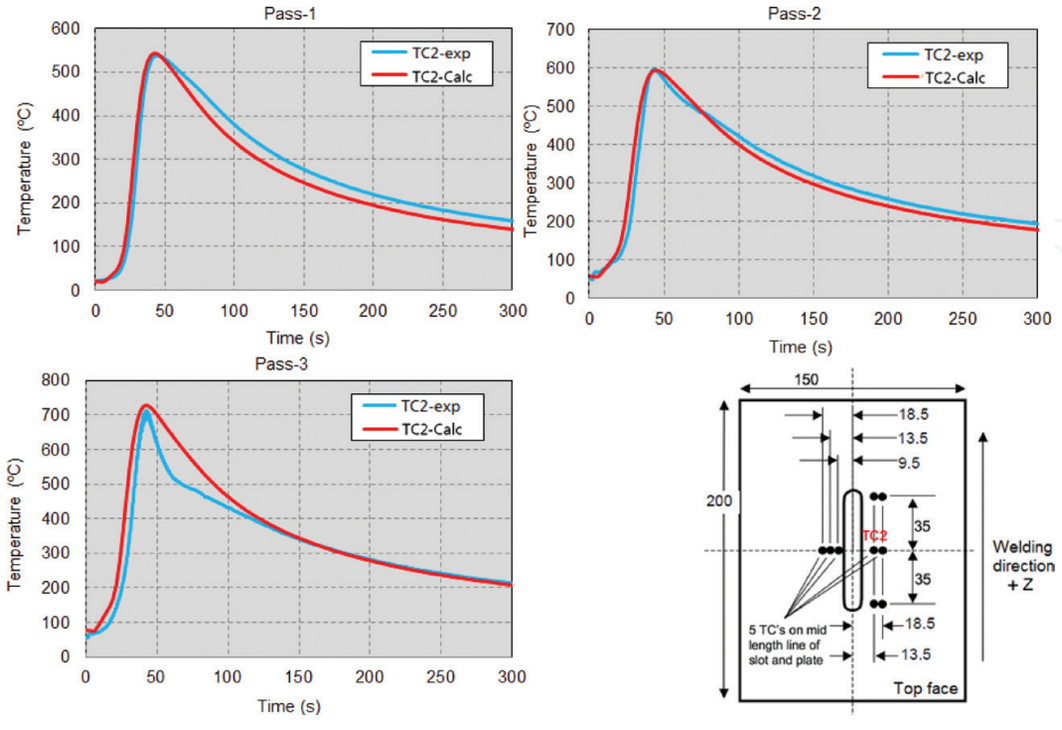

Figure 15. Experimental and numerical temperature histories for three-pass slot weld at mid-length thermocouple TC2.

http://dx.doi.org/10.5772/intechopen.74466

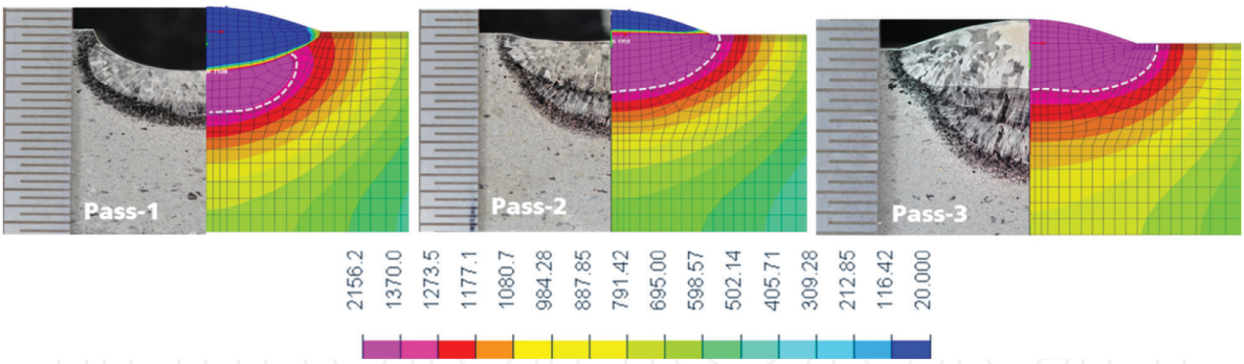

Figure 16. Calculated temperature contour plots of three weld passes compared with the real fusion boundaries.

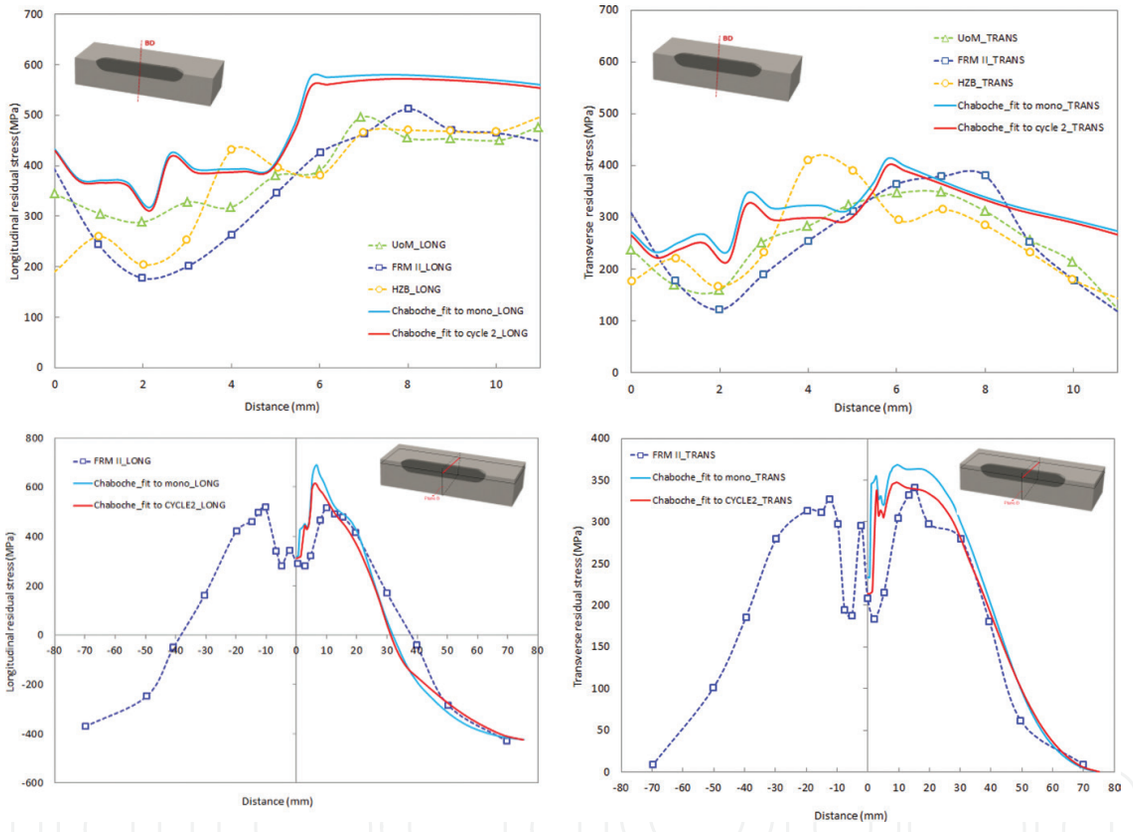

Figure 17. Comparison between the measured and calculated residual stress components on lines BD (top) and B2 (bottom).

3. Conclusions

In this chapter, three welding simulation case studies were reviewed. As the first case study, the numerical analysis of welding residual stresses in single bead tubular specimens made of structural steel S355J2H was studied. In case study 2, the NeT Task Group 1 was reviewed which focuses on single-pass weld bead on plate made of AISI 316 L and for case study 3, the NeT Task Group 6 was considered which is about the three-pass slot welds of nickel alloys. There exist very well documented experimental results on tubular specimens made of S355J2H in the project DFG FA992/1–1. On the other hand, NeT projects include a

wide range of experimental measurements parallel to its advanced simulation programs. The goal is to develop a comprehensive simulation methodology for the prediction of residual stresses under the assistance of precise measurement techniques. Based on the results and achievements, FE simulation could be applied as a powerful tool for predicting the welding residual stresses required for the integrity assessments. The summaries of all these efforts have been already released in terms of a couple of recommendations. Exact thermal solutions, use of advanced material hardening models and including high-temperature annealing effects are some of the most important items out of those recommendations.

The key conclusions and findings in this period are listed as follows:

1. Welding residual stresses within the tubular welded joint could be accurately determined by means of the numerical simulation approach considering the phase transformations, microstructure- and temperature-dependent mechanical properties, transformation-induced plasticity and recovering of strain hardening during transformation.
2. Combining the residual stress measurement results from X-ray and neutron diffraction over the whole cross section of welds showed a sharp gradient in the welding residual stress profile from top surface toward the material bulk.
3. Based on the simulations of the tubular welds, the material in the weld area undergoes compressive stresses due to the $\gamma \rightarrow \alpha$ transformation-induced expansions during cooling.
4. For the material S355J2H, isotropic hardening model seems to be suitable for predicting welding residual stresses.
5. In welding simulation, before proceeding to mechanical simulation, a verified global heat input and a calibrated heat source is absolutely necessary.
6. The use of kinematic and combined hardening models or preferably elasto-viscoplastic material constitutive behavior is recommended for the welding simulation of stainless steel and Inconel.
7. The used material constitutive model for the weld metal could differ from that of base material.

Acknowledgements

This contribution was partially supported by the German Research Foundation (Deutsche Forschungsgemeinschaft – DFG) as part of the projects DFG FA992/2-1 “Numerical description of the behavior of welding residual stress field under multiaxial mechanical loading” and DFG FA992/2-2 “Numerical Incorporation of the Damaging Effects of Residual Stresses in the Multiaxial Fatigue Assessment of Welded Components and Structures”. The respective residual stress measurements were done at the Helmholtz-Zentrum Berlin (HZB) and the Forschungs-Neutronenquelle Heinz Maier-Leibnitz (FRM II) in Munich, Germany. The authors would like to thank deeply for the support. For those experiments conducted within the activities of NeT (Network on Neutron Techniques standardization for Structural Integrity) round robin, the authors would like to use the opportunity to express their gratitude to everyone who was involved in this fruitful collaboration.

Author details

Kimiya Hemmesi and Majid Farajian*

*Address all correspondence to: majid.farajian@iwm.fraunhofer.de

Fraunhofer Institute for Mechanics of Materials IWM, Germany

References

[1] R6. Assessment of the Integrity of Structures Containing Defects. Br. Energy. Revision 4; 2013

[2] Farajian M, Nitschke-Pagel T, Wimpory RC, Hofmann M, Klaus M. Residual stress field measurements in welds by means of X-ray, synchrotron and neutron diffraction. Journal of Materials Science and Engineering Technology. 2011;**42**(11):996-1001

[3] Boulton NS, Lance Martin HE. Residual stresses in arc-welded plates. Proceedings of the Institution of Mechanical Engineers. 1936;**133**:295-347

[4] Rosenthal D. Mathematical theory and heat distribution during welding and cutting. Welding Journal. 1941;**20**(5):220-234

[5] Goldak JA, Akhlaghi M. Computational Welding Mechanics. New York, USA: Springer; 2005. ISBN-10:0-387-23287-7

[6] Radaj D. Eigenspannungen und Verzug beim Schweißen, Rechen- und Messverfahren. Fachbuchreihe Schweißtechnik. Düsseldorf: DVS-Verlag GmbH; 2000

[7] Goldak J. Web based simulation of welding and welded structures. CWA Conference. 2013

[8] Hemmesi K, Farajian M, Boin M. Numerical studies of welding residual stress field in tubular joints and the related experimental investigations by means of X-ray and neutron diffraction analysis. Materials and Design. 2017;**126**:339-350

[9] Farajian M. Residual stress relaxation in high strength steel welded joints under multiaxial loading. DFG-FA992/1-1 Final Report. 2015

[10] Smith MC, Smith AC, Wimpory R, Ohms C. A review of the NeT Task Group 1 residual stress measurement and analysis round robin on a single weld bead-on-plate specimen. International Journal of Pressure Vessels and Piping. 2014;**120-121**:93-140

[11] Smith MC. NeT TG6 Finite Element Simulation Protocol, Issue 1 for Phase 1 Simulations, 2016

[12] Farajian M. Stability and relaxation of welding residual stresses [PhD dissertation]. Braunschweig, Germany: Shaker Verlag; 2011

[13] Armstrong PJ, Frederick CO. A mathematical representation of the multiaxial bauschinger effect. CEGB Report RD/B/N731. 1966

[14] Goldak J, Chakravariti A, Bibby M. A new finite element model for welding heat sources. Metallurgical Transactions. 1984;**15B**:299-305

IntechOpen